

# Wide-field near-infrared all-reflecting camera with Fabry-Perot for astronomy

Yin-sheng Sun

Michael C. B. Ashley

John W. V. Storey

School of Physics, University of New South Wales  
Sydney 2052, Australia

## ABSTRACT

We describe the specifications and design of a  $1\text{--}5\ \mu\text{m}$  camera (IRC-UNSW) being built at the School of Physics, University of New South Wales, for use on the 4-m Anglo-Australian Telescope (AAT) and the 2.3-m telescope of the Australian National University. The camera design uses three off-axis mirrors, allowing it to correct the off-axis aberrations in the telescopes themselves, and to obtain images with FWHM blur circles of  $10\ \mu\text{m}$  over a wide field-of-view ( $4.5\times 4.5$  arcmin on the AAT,  $5.8\times 5.8$  on the 2.3-m). The camera accepts a collimated beam and can be used with an external Fabry-Perot etalon. We have fully characterised the performance of the camera with respect to misalignment and manufacturing errors. A thermal model has allowed us to calculate cool-down times, cryogen usage, and distortion due to small temperature differences in the optical system.

**Keywords:** Fabry-Perot etalon, reflecting, near-infrared, imaging, astronomy

## 1 INTRODUCTION

Our goal is to build a camera that can acquire near-infrared images of astronomical objects at spectral resolving powers of up to 3000 or greater over a wide field. This dictated the use of a Fabry-Perot etalon with a large clear aperture placed in a collimated beam. While it is not strictly necessary for the etalon to be in a collimated beam, it allows the highest possible spectral resolution to be achieved. This set the basic parameters of the camera.

We designed IRC-UNSW to use all-reflective optics. The advantages of such a system—fewer ghost reflections, higher transmission, and no chromatic aberration—are well known. By using three off-axis mirrors we have been able to control the aberrations over a wide field and arrive at a satisfactory design that meets all our requirements.

It became clear early in the design process that the aberrations of the telescope itself could not be ignored.

Although the AAT is a Ritchey-Chretien design with a nominal field diameter of 40 arcminutes, the telescope is only coma-free when the  $f/8$  top-end is used.<sup>1</sup> This top-end is unsuitable for infrared astronomy because of the obscuration of the large secondary mirror. When the telescope is used with the  $f/15$  infrared secondary the Ritchey-Chretien criterion is not satisfied, and there is significant coma a couple of arcminutes off-axis. We therefore optimised the design with all the telescope optics included. The original design<sup>2</sup> was done for the AAT alone, however we have since been able to produce a single design that is compatible with both the AAT and 2.3-m telescopes simply by moving the collimator mirror. The FWHM blur circle on the 2.3-m is  $30\ \mu\text{m}$ .

This paper reports a detailed description of the opto-mechanical design of the camera. A brief description of the configuration and performance of the camera imaging system (section 2) will be followed by a discussion of the sensitivity of the system to misalignment and manufacture errors (section 3). In section 4 we present the detailed drawings of the optical structure, in section 5 the thermal analysis, and in section 6 describe the Fabry-Perot etalon.

The camera is currently being constructed in the workshops of the School of Physics, UNSW, with a contract for the optics being let in July 1995. The Fabry-Perot was delivered in early 1995 and is being commissioned with the IRIS camera<sup>3</sup> on the AAT.

## 2 OPTICAL CONFIGURATION AND PERFORMANCE

### 2.1 General description

The purpose of the optics in a near-infrared astronomical camera is to (a) reduce the image scale of the telescope to match available detector arrays, and (b) baffle the detector from unwanted internal and external infrared radiation.

Figure 1 shows the optical layout of our camera design. The convergent beam ( $f/15$  for the AAT,  $f/18$  for the 2.3-m) from the telescope forms an image at the focal plane, as shown at the top of the Figure. Due to space limitations it is necessary to introduce a flat mirror to fold the optical path before it strikes the spherical collimating mirror. The collimator images the telescope's pupil (the secondary mirror for Cassegrain configurations) at a stop within the camera in order to eliminate stray infrared radiation. The Fabry-Perot etalon is placed as close as possible to this stop, thereby minimizing its required diameter (70 mm in this design).

After passing through the Fabry-Perot, the beam strikes a calcium fluoride entrance window before entering the evacuated space containing the off-axis three-mirror imaging system, as shown in the bottom of Figure 1. The mirrors produce a re-imaged focal plane on the detector array with a final focal ratio of  $f/3.5$ . A flat mirror is used to fold the optical axis for convenience prior to passing through one of several 1% filters used to remove unwanted orders transmitted by the Fabry-Perot. After the Fabry-Perot and entrance window, all the optical components are cooled to 77 K with liquid nitrogen to reduce thermal emission.

Figure 2 is an exploded view of the optics box.

### 2.2 Design optimization

Due to the asymmetry of the off-axis mirror system, the distribution of its image quality over the whole field of view is quite different from a symmetrical system.<sup>4-8</sup> The traditional method of optimization using the meridian plane is not adequate. We chose a grid of 9 points on the image plane, and minimized the sum of the

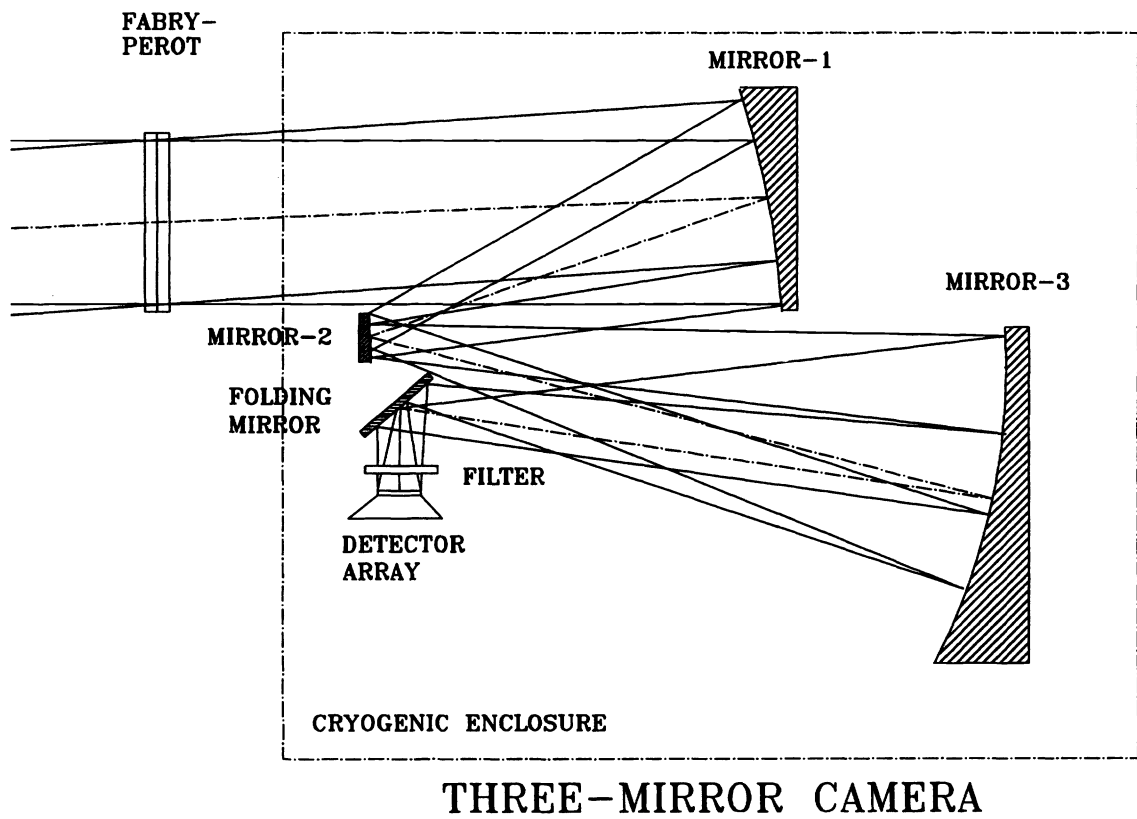
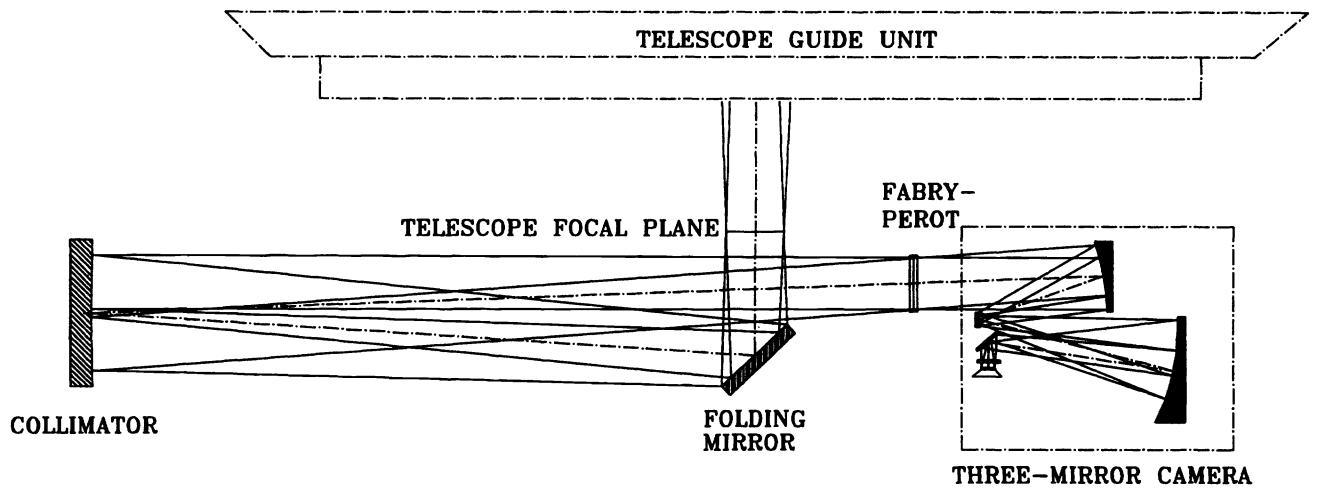


Figure 1. The overall optical layout of the camera.

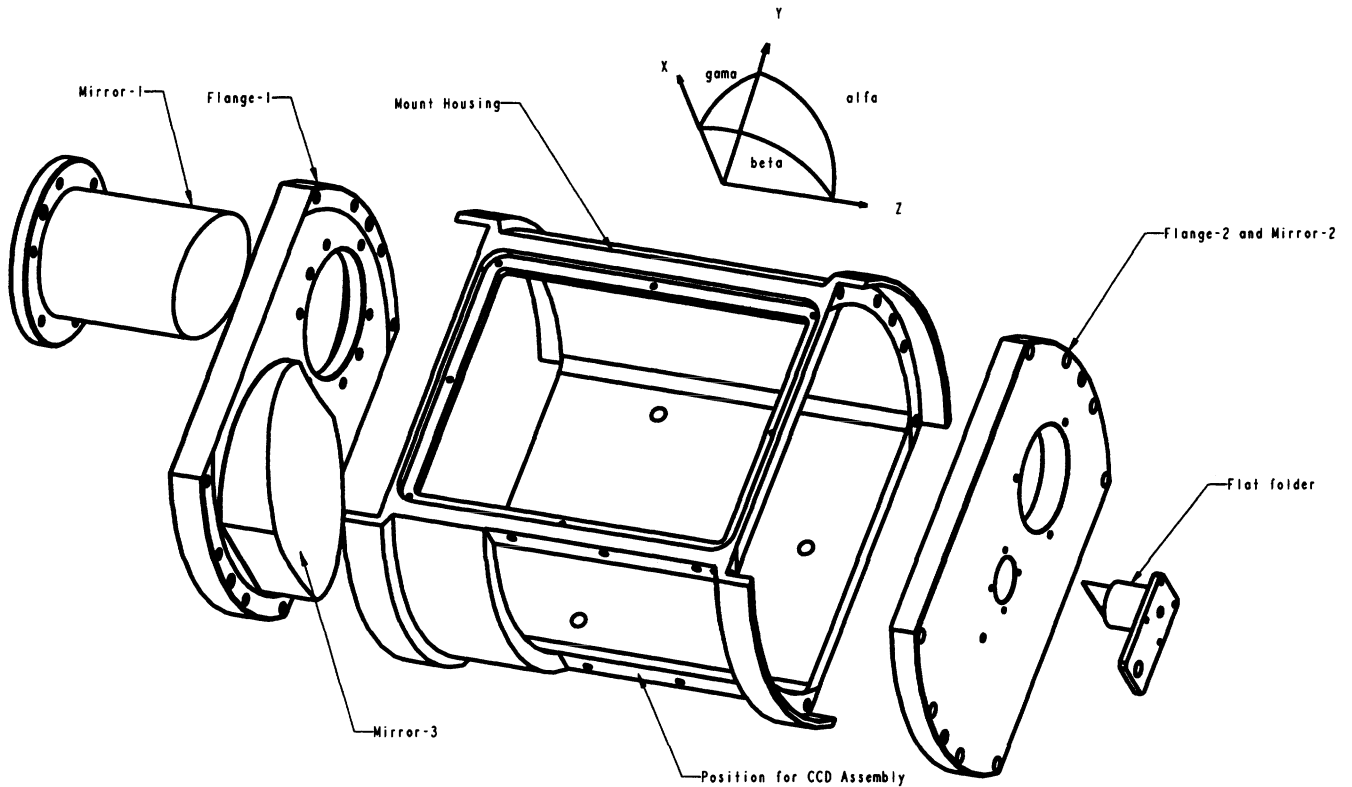


Figure 2. An exploded view of the optics box, showing the coordinate system used in ray-tracing. A liquid nitrogen container bolts to the lower flat surface of the "Mount Housing".

squares of the spot diameters. Any short-cuts, such as using a cross-shaped pattern of points rather than a grid, led to large aberrations at points away from those optimized.

By including all optical elements (the primary and secondary mirrors of the telescope, as well as the tilted collimator) we were able to successfully balance the aberrations of the telescope and IRC-UNSW and thereby produce images limited only by the detector's pixel size, throughout the image plane.

Figure 3 shows the distribution of the root-mean-square optical path difference (RMSOPD), and Figure 4 shows the spot diagrams over the whole field of view. The image plane covers  $17.6 \times 17.6$  mm, allowing large-format array detectors to be used.

Table 1 summarizes the main specifications for the camera, and Table 2 gives the final optical design parameters.

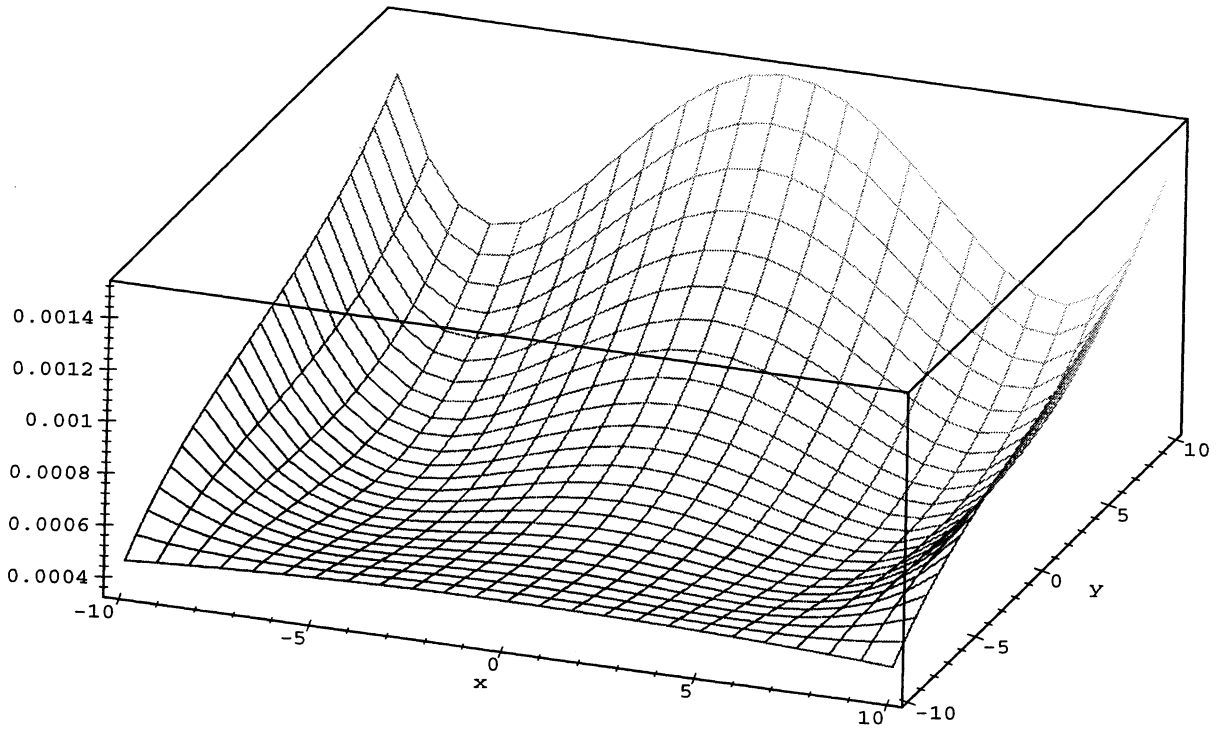


Figure 3. The distribution of the RMS optical path difference in the image plane. All dimensions are in millimetres.

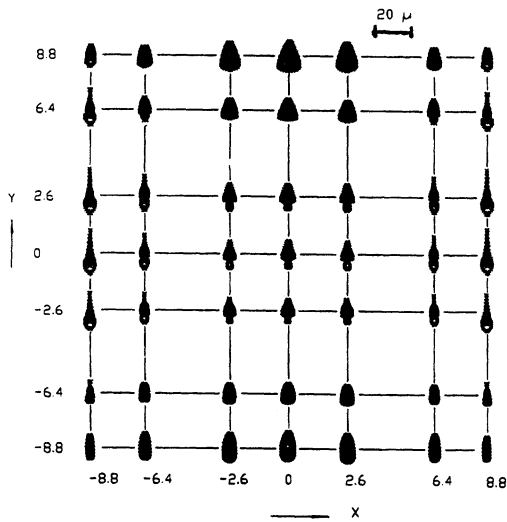


Figure 4. The variation in spot size as a function of position on the image plane. Dimensions in millimetres. A 20 μm scale bar is shown at top right.

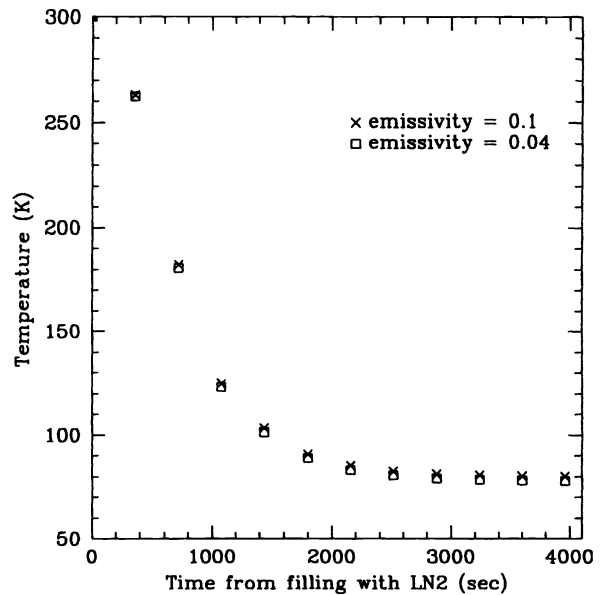


Figure 5. The cool-down time of the camera for two different emissivities of the components.

Table 1. Main specifications of the camera.

Parameter	AAT value	2.3-m value
Field of view	267×267 arcsec	350×350 arcsec
Pixel projection on the sky†	~0.5 arcsec	~0.7 arcsec
f-number of telescope	f/15	f/18
f-number of camera		f/3.5
Spectral coverage		1–5 μm
Maximum detector area		17.6×17.6 mm
Optics		Off-axis reflective system
Spectrometer		Fabry-Perot etalon, coated for 1.5–2.5 μm
Spectral resolving power		$\lambda/\Delta\lambda = 3000$
Broad-band filters		Astronomical J, H, K, L'
Narrow-band filters		Provision for 7 narrow-band filters
Cooling		Optics at 77 K; detector from 15–77 K

† With the 512×512-pixel PtSi detector from Mitsubishi.<sup>9,10</sup> Value given are the average for the two sides of the 20×26 μm pixels.

Table 2. Parameters of the optical system, at operating temperature (77 K).

Surface	Radius Curv.		Separation mm	Conic constants	Aspheric coefficients	
	mm	mm			A4	A6
1 AAT primary	-25400.00		0.0	-1.1717		
2 AAT secondary	-6722.00		-10077.0	-4.1882		
3 AAT flat	+0.00		+12345.8	+0.00		
4 AAT collimator	-1960.0		+600	+0.00		
1 2.3-m primary	-9600.0		0.00	-1.00		
2 2.3-m secondary	-1356.52		-4200.0	-1.58979		
3 2.3-m flat	+0.00		+5497.6	+0.00		
4 2.3-m collimator	-1960.0		+650	+0.00		
5 (mirror 1)	-354.54		+1235.59	-0.68773		
6 (mirror 2)	-146.04		-167.02	-6.27081		
7 (mirror 3)	-252.32		+248.60	-0.06084	-4.41E-11	-3.61E-15
8 (detector)	+0.00		-270.75	+0.00		

## 2.3 The detector

During the commissioning phase of the instrument we will be using a 512×512-pixel platinum silicide array detector manufactured by Mitsubishi,<sup>9,10</sup> and driven by electronics developed in-house.<sup>11</sup> Other detectors can be swapped in, and cooled to temperatures between 15 K and 77 K using a closed-cycle cooler.

### 3 EFFECTS OF MISALIGNMENT AND MANUFACTURING ERRORS

For ease of manufacture and ease of use, we elected to have no provision for adjusting the positions and tilts of the cryogenic mirrors or the detector. To test whether this was feasible, we thoroughly investigated the effects on image quality of misalignment and manufacturing errors. We used a Cartesian coordinate system,  $x$ ,  $y$ ,  $z$ , for each optical element, with the  $+z$  axis defined as the direction of propagation along the optical axis, and the  $x$  axis coming out of the page in Figure 2. An off-axis mirror can be misaligned with respect to 6 degrees of freedom: translations along  $x$ ,  $y$ ,  $z$ , and rotations  $\alpha$ ,  $\beta$ ,  $\gamma$ , about these axes.

We used the RMS optical path difference as a merit function, and found empirically that if this was less than  $0.7\ \mu\text{m}$ , good image quality would be obtained. Figure 6 shows the variation in the RMS OPD on axis as a function of misalignments of the mirrors, and of manufacturing errors in the shape of the surfaces. Note that the minima do not always correspond exactly with misalignments of zero; this is because Figure 6 is for the on-axis point, whereas we optimised the design for the best results over the image plane.

In summary:

1. The position of mirror 1 is the most critical: its  $x$  position must be held to within  $\pm 0.1\ \text{mm}$ , and its  $\beta$  rotation to  $\pm 0.02^\circ$ . Mirror 1 is also the most sensitive to surface errors: the radius must be held within  $\pm 0.1\%$ , and the conic constant within ( $\pm 0.005\%$ ).
2. The system is relatively insensitive to misalignment and surface errors in mirror 2.

### 4 OPTO-MECHANICAL STRUCTURE AND DIAMOND TURNED OPTICS

In designing the mechanical structure to support the optical surfaces we were guided by three requirements:

1. All optical surfaces should be held accurately within the tolerances found in the preceding section. Any adjustments should be easy to perform.
2. The detector array should be well shielded from unwanted thermal radiation.
3. No distortion of the structure, apart from linear shrinkage, should occur when it is cooled to  $77\ \text{K}$ .

Traditionally, off-axis mirror systems have required accurate alignment after manufacture,<sup>12</sup> whereas co-axial lens systems often can be built with no provision for adjustment.<sup>13,14</sup> Given the difficulty of aligning at cryogenic temperatures the 15 degrees of freedom in our three-mirror design adjustments, we have designed an optics box that can be machined out of a single piece of aluminium using single point diamond turning (SPDT), with zero degrees of freedom. For near-infrared imaging systems, the mirror surface accuracies and finishes from SPDT can be quite acceptable.<sup>15-18</sup>

To minimise the number of separate components, there are only three main parts to the structure (see Figure 2): a flange holding mirrors 1 and 3, a flange holding mirror 2, and an optical housing. To achieve uniformity of thermal properties and to create a satisfactory surface finish, all parts are made of T-6061 aluminium (or Alumec 89, which takes a better finish). The optical housing has an oval cross section to reduce its weight and volume. Its two end faces are turned out by SPDT to allow highly accurate alignment with the two end flanges. For ease of manufacture, mirror 1 is designed to be a sub-assembly on mirror 3, since otherwise the diamond tool would strike the surface of mirror 1 while the mirror 3 surface was being turned. After mirror 3

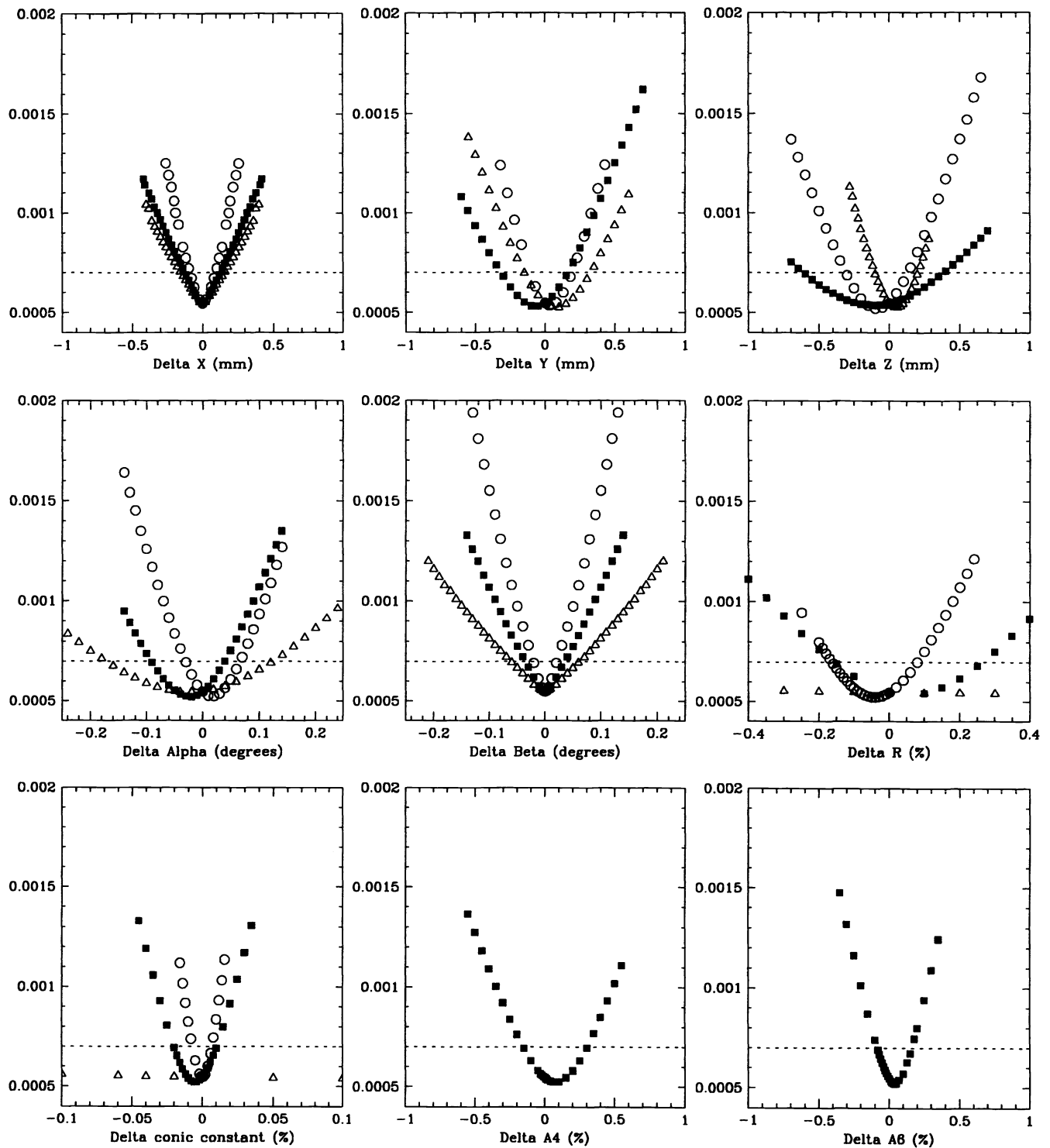


Figure 6. The effect of various types of manufacturing errors on the RMS optical path difference on axis. The open circles are for Mirror 1, the open triangles are for Mirror 2, and the filled squares are for Mirror 3. The dashed line represents the acceptable limit of the RMS OPD in order to obtain good images.

has been machined, mirror 1 is mounted in position and surface turned by SPDT. The precision with which it can be placed is about  $\pm 0.005$  mm which is adequate given the calculated allowable tolerance in the positioning of mirror 1. For the minimum system aberration, the three mirrors are not only off-axis but non-coaxial. The most sensitive to alignment is mirror 3, so we choose its axis as the interface assembly axis. The radial location of the three components is determined by machined surfaces. The accuracy to which SPDT can control diameters is typically 0.002 mm. The mounting surfaces on mirror 2 and mirror 3 are designed to be on the same sides as their mirror surfaces, in order that they can be machined in the same operation to high accuracy. The SPDT mounting surfaces precisely control the tilt and separation of the two mirrors. Two precision dowels constrain the rotation of the mirrors about the  $z$  axis. The two mirror flanges are mounted into the housing, using a similar radial location method to that used for the mirrors themselves.

## 5 THERMAL ANALYSIS WITH FEM

In order to reduce the thermal background, most infrared imaging systems are operated at low temperature. In IRC-UNSW, the three-mirror imaging system is operated at 77 K, while the detector can be run at anywhere between 15 K and 77 K. However, the telescope, folding flat and collimator mirror are all at room temperature. Careful thermal analysis is therefore necessary to assess the effect of these large temperature differences on the optical performance of the system as a whole. This thermal analysis also enables us to predict cool-down time and coolant consumption under a variety of assumptions.

The Finite Element Method (FEM) is an economical, reliable and accurate tool for analysing the thermal behaviour of infrared optical systems, and has been used widely in cryogenic optical design.<sup>19-22</sup> The analysis described in this paper was carried out with MSC/NASTRAN.

The analysis begins with the creation of a detailed mesh-structure model and providing NASTRAN with the appropriate material properties. The mesh was created by MSC/XL, and the analysis was performed on an IBM RS6000 workstation. The optical housing is attached under the LN2 tank, and has mirror flanges at each end. The complete mesh model consists of 3235 grid points and 1487 elements (QUAD4, TRI3, HEXA, and PENTA). For greatest accuracy, the density of the grid points on the mirror surfaces is set higher than the density on the other surfaces. The thermal radiation energy input to each grid point from the surfaces facing it was calculated, taking into account the assumed emissivity of those surfaces.

Figure 5 shows how the optics box cools from the instant at which liquid nitrogen is poured into the can. The temperature plotted is the average of the temperatures of the centers of the two flanges. The main results are:

1. The mirror system will take an hour to cool down from room temperature to 80 K, and it takes another hour to reach a stable temperature of 77.89 K (assuming an emissivity of 0.04).
2. The cool-down time is fairly independent of emissivity. However, the final equilibrium temperature reached depends significantly on the emissivity, rising from 77.89 K to 80 K if the emissivity changes from 0.04 to 0.1.

Another effect of the higher emissivity is, of course, coolant consumption. With an emissivity of 0.04, the LN2 consumption is 25 liters for cool-down and 0.25 liters/hour to keep the optics cold. With the emissivity increased to 0.1, the LN2 consumption will be  $\sim 0.7$  liters/hour. Highly polished surfaces and the use of super-insulation can reduce the emissivity to very small values.

## 5.1 Thermal distortion of the mirror surfaces

In IRC-UNSW, the camera system and telescope operate at different temperatures: 77 K and 300 K respectively. Since the optical optimisation of IRC-UNSW was carried on the system as a whole, but only the camera is to be cooled, we were interested in knowing how the cool-down would affect image quality. In addition, by modelling the differing thermal loads on the optical box using NASTRAN, we were able to determine the resultant small temperature differences across the structure. Assuming an emissivity of 0.04 for the exterior surfaces of the optics box, a maximum temperature differential of 2.0°C is present, causing a small deformation in the optical surfaces. We then took the zernike coefficients from NASTRAN and converted them into the usual ray-tracing conic constants and aspheric coefficients. We are continuing our investigations into this problem.

## 6 THE FABRY-PEROT ETALON

The 70 mm diameter Fabry-Perot etalon is a type EC70-WF, manufactured by Queensgate Instruments in the UK. The etalon plates are of water-free silica, and have a multilayer coating that covers the range 1.5 to 2.5  $\mu\text{m}$ , with a nominal finesse of around 60. Operating in 50th order at 2.12  $\mu\text{m}$ , the etalon delivers a resolving power of approximately 3,000.

Because the Fabry-Perot is operating in a collimated beam, it alone determines the spectral resolution. At a later stage, we can replace the existing etalon and achieve much higher resolutions. The disadvantage of placing the etalon in the pupil plane is that the transmitted wavelength varies as a function of radial distance from the centre of the field. This effect is minimised by using a large-diameter etalon, so that the ray bundles for the off-axis pixels are at only a small angle to the optical axis.<sup>23</sup>

## 7 ACKNOWLEDGEMENTS

We are grateful to Shuji Sato of the National Astronomical Observatory, Japan, for providing the PtSi detector. John Isles, of the School of Mechanical Engineering, UNSW, provided invaluable assistance with the use of CAD and FEM computing packages. We thank the staff of the Mechanical Workshop in the School of Physics, UNSW, for their outstanding efforts in constructing IRC-UNSW. We acknowledge financial support from the Australian Research Council.

## 8 REFERENCES

- [1] J. W. V. Storey (ed). "Anglo-Australian Observatory Observers' Guide," 1981.
- [2] Y. Sun, M. C. B. Ashley and J. W. V. Storey. "A new infrared camera optical design," *Proc. ASA*, **10**, 137, 1992.
- [3] P. Gillingham and A. Lankshear. "An infrared array camera/spectrometer for the Anglo-Australian Telescope," *SPIE*, **1235**, 1990.
- [4] P. N. Robb. "Three-mirror telescopes: design and optimization," *Appl. Opt.*, **17**, 2677, 1978.
- [5] D. R. Shafer. "Four-mirror unobstructed anastigmatic telescopes with all-spherical surfaces," *Appl. Opt.*, **17**, 1072, 1978.

- [6] R. E. Fisher. "Lens design for the infrared," *SPIE Critical Reviews*, Vol. CR38, 19, 1991.
- [7] D. Korsch. "Design and optimization technique for three-mirror telescopes," *Appl. Opt.*, **19**, 3640, 1980.
- [8] J. W. Figoski. "Aberration characteristics of nonsymmetric systems," *SPIE*, **554**, 104, 1985.
- [9] M. Kimata, M. Denda, N. Yutani, S. Iwade and N. Tsubouchi. "A 512x512 element PtSi Schottky-barrier infrared image sensor," *ISSCC Tech. Digest*, 110, 1987.
- [10] N. Yutani, H. Yagi, M. Kimata, J. Nakamishi and N. Tsubouchi. "1040x1040 element PtSi Schottky-barrier IR image sensor," *IEDM Tech. Digest*, 175, 1991.
- [11] M. H. Unewisse, D. I. Iordanescu, A. Brocklesby, K. S. Bentley, and J. W. V. Storey. "A general control system for imaging arrays", *Measurement Science and Technology*, **5**, 347, 1994.
- [12] J. W. Figoski, T. E. Shrode and G. F. Moore. "Computer-aided alignment of a wide-field, three-mirror, unobscured, high-resolution sensor," *SPIE*, **1049**, 166, 1989.
- [13] I. S. McLean, T. C. Chuter, M. J. McCaughrean and J. T. Rayner. "System design of a 1-5  $\mu\text{m}$  IR camera for astronomy," *SPIE*, **627**, 430, 1986.
- [14] I. M. Egdall. "Manufacture of a three-mirror wide-field optical system," *Opt. Eng.*, **24(2)**, 285, 1985.
- [15] R. A. Clark. "Design and specification of diamond turned optics," *SPIE Critical Reviews*, Vol. CR38, 164, 1991.
- [16] J. K. Myler, R. A. Parker and A. B. Harrison. "Advanced optical manufacturing and testing," *SPIE*, **1333**, 58, 1990.
- [17] M. C. Gerchman. "Specifications and manufacturing considerations of diamond machined optical components," *SPIE*, **607**, 36, 1986.
- [18] H. G. Sillitto. "Analysis, tolerancing and diagnosis of diamond machining errors," *SPIE*, **1013**, 105, 1988.
- [19] C. D. Theim. "Finite element analysis enhancement of cryogenic testing," *SPIE*, **1532**, 39, 1991.
- [20] S. Weinswig and R. A. Hookman. "Optical analysis of thermal induced structural distortions," *SPIE*, **1527**, 118, 1991.
- [21] A. E. Hatheway. "An overview of the finite element method in optical systems," *SPIE*, **1532**, 2, 1991.
- [22] W. R. Powell. "Analysis of thermal stability of fused optical structures," *SPIE*, **1532**, 126, 1991.
- [23] P. D. Atherton, N. K. Reay and J. Ring. "Tunable Fabry-Perot filters," *Opt. Eng.*, **20**, 806, 1981.